Nondestructive characterization of a TiN metal gate: Chemical and structural properties by means of standing-wave hard x-ray photoemission spectroscopy

C. Papp,[1,a)] G. Conti,[1] B. Balke,[1,b)] S. Ueda,[2] Y. Yamashita,[2] H. Yoshikawa,[2] Y. S. Uritsky,[3] K. Kobayashi,[2] and C. S. Fadley[1]
[1]*Materials Sciences Division, Lawrence Berkeley National Laboratory, One Cyclotron Road, Berkeley, California 94720, USA and Department of Physics, University of California, One Shields Avenue, Davis, California 95616, USA*
[2]*NIMS Beamline Station at SPring8, National Institute for Materials Science, 1-1-1 Kouto, Sayo, Hyogo 679-5148, Japan*
[3]*Applied Materials, Inc., 3050 Bowers Avenue, Santa Clara, California 95054, USA*

(Received 21 July 2012; accepted 17 October 2012; published online 3 December 2012)

Standing-wave (SW) hard x-ray photoemission (HXPS, HAXPES) is applied to a thick (100 Å) film of a metal gate TiN grown on top of a Si/$MoSi_2$ multilayer mirror. The mirror is used to produce a standing wave of 30 Å period that is scanned through the sample by varying the x-ray incidence angle over its 1st-order Bragg condition, thus generating rocking curves of various core-level intensities. The thickness and chemical state of the top, oxidized surface of TiN, as well as the buried interface between TiN and the native oxide on top of the mirror are determined by SW-HXPS. The information provided by SW-HXPS is compared to that obtained by XPS Ar^+ depth profile. The SW-HXPS method not only does not require destroying the sample but also provides more quantitative results and a more detailed profile of the interfaces than XPS Ar^+ depth profile. Various applications of SW-HXPS to nanoscale multilayer semiconductor systems are thus suggested. © *2012 American Institute of Physics*. [http://dx.doi.org/10.1063/1.4765720]

I. INTRODUCTION

Titanium nitride (TiN) is a multifunctional compound that is used in many technologically relevant areas.[1,2] The multiple uses of TiN, which is part of the family of early transition metal nitrides, stem from their exceptional properties: they have a high thermal and electrical conductivity, which is comparable to metals. Additionally they are brittle, very hard, and show a high melting point. Due to the wear and corrosion resistance of TiN, it is used as a protective coating on metals, including tools used for surgery and various high speed cutting applications. For instance, TiN coatings with thicknesses of about 2–10 μm are generally found to increase tool life by several hundred per cent.[1]

TiN also has important applications in the semiconductor microelectronics industry.[2] It is used as a diffusion barrier in contact structures, both to prevent Cu diffusion into the nearby dielectric material and to provide an adhesive layer for improving the adhesion of the dielectric material to Cu. With the progressive scaling down of semiconductor devices, new gate materials are also needed to fulfill more stringent device requirements such as low gate leakage currents and adequate electrical performance. The replacement of the traditionally used SiO_x dielectric with materials of higher dielectric constant such as Hf-based films has also required the augmentation of doped poly-Si gates with more suitable materials (M1 in the generic CMOS gate shown in Figure 1). TiN is thus under evaluation as a potential gate electrode for sub 32 nm node device applications.[3]

In view of the very small thicknesses of the gate materials (at present dielectrics of ≈10 Å, and metal gates of (M1) ≈100 Å), the surface and buried interface properties are critical to ultimate performance. Even though TiN is stable over a broad composition range, its structure and properties depend critically on its actual composition. Physical properties such as electrical resistivity depend strongly on film stoichiometry and morphology. For instance, the presence of oxygen and/or carbon in the film results in low hardness and high resistivity, which does not meet the stringent requirements of semiconductor technology. One important reaction is that of oxygen from the surface or buried interfaces, which can yield a resulting layer composed of titanium oxynitride (TiON); this is thus an important species to determine.[4,5] It is also important to characterize the TiN/SiOx interface in order to determine if the deposition of TiN has reduced the silicon oxide layer and generated an interface rich in Si and/or a TiON or $TiSi_x$ layer.

In this paper, we study a TiN film deposited by a physical vapor deposition (PVD) process as a potential metal gate electrode in the 32 nm technology node and beyond. Figure 1 shows a schematic of: (a) a typical CMOS gate structure and (b) the nominal configuration of the analyzed sample. The characterization of the TiN film in terms of composition, and the depth distribution of different chemical species through its interfaces has been performed by combining soft x-ray (SXPS at ≈1.5 keV) and hard x-ray photoelectron spectroscopy (HXPS or HAXPES at ≈6 keV). In particular, we focus our attention on the characterization capabilities of the newly

[a)]Present address: Lehrstuhl für Physikalische Chemie II, Universität Erlangen-Nürnberg, 91058 Erlangen, Germany.
[b)]Present address: Institut für Anorganische und Analytische Chemie, Johannes Gutenberg-Universität, 55099 Mainz, Germany.

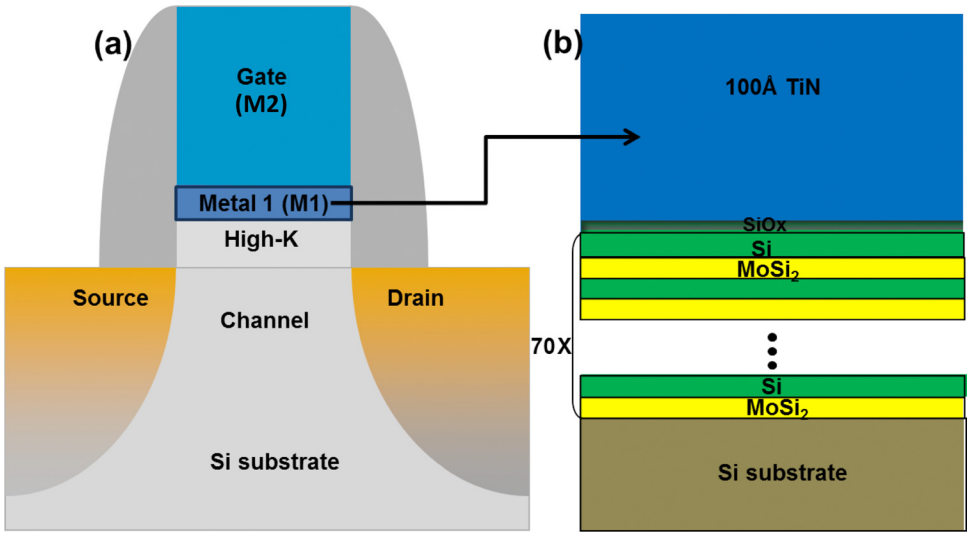

FIG. 1. (a) Schematic of a typical CMOS gate structure with two metallic gate materials, (b) the nominal geometry of our sample: 100 Å TiN grown on top of a $Si/MoSi_2$ multilayer with period 25.5 Å Si + 4.5 Å $MoSi_2$.

developed technique of standing-wave (SW) x-ray photoemission, as extended into the hard x-ray regime (SW-HXPS).[6–9]

As noted above, the thickness of a typical metal gate (M1) film is in the range of 100 Å. Films of such a thickness in the range of 100–200 Å are ideal candidates for SW-HXPS applications, and in fact cannot be fully characterized neither by SXPS of the type normally available in analytical laboratories nor by other surface-sensitive and non-destructive techniques. More precisely, SXPS with excitation energies up to about 1.5 keV cannot reach the 100 Å depth due to the electron inelastic mean free paths (IMFPs) that are at most a few tens of Å. In hard x-ray photoemission at about 6 keV the IMFPs are 3–4 times as large, enabling the study of deeply buried layers and interfaces. Some IMFP estimates at 6 keV for the materials in our sample from the TPP-2M approach[10–12] are: TiN ≈ 81 Å, Si ≈103 Å, and Mo ≈ 69 Å.

Another common method of accessing information regarding such a deep interface is XPS Ar^+ sputter depth profile, which necessarily destroys the sample and is subject to the problems associated with sputtering (preferential sputtering, knock off, etc.), thus potentially leading to false concentration profiles and unreliable chemical-state information of the species involved. Additionally, the process of sputtering induces intermixing of the layered structures, thus limiting information of the "real" diffusion that might exist at the interfaces.[13] The preparation procedures for growing TiN have been studied extensively.[14–20] These studies include characterization by XPS Ar^+ sputter profiling and thus permit comparisons to the data we have obtained using HXPS for the same sample preparation procedure.[21–23]

In order to quantitatively access the deeply buried TiN/SiO_x/Si interfaces in our sample, we use SW-HXPS. The standing wave allows us to tune the electrical field of the x-rays to be specifically enhanced at different depths in the sample. As noted, the greater kinetic energy of photoelectrons in hard x-ray experiments (up to ≈ 6 keV) leads to a larger electron escape depth >80 Å;[10–12] thus, information on deeply buried interfaces can be recorded and analyzed in a non-destructive manner. The SW aspect of the technique is based on the spectroscopic analysis of photoelectrons excited by a strong standing wave which originates inside a synthetic multilayer mirror[24] at the incidence angle defined by the first-order Bragg condition $\lambda_x = 2d_{ML}\sin\theta_{inc}$, where λ_x is the incident photon wavelength, d_{ML} is the period of the multilayer mirror, and $\sin\theta_{inc}$ is the grazing x-ray incidence angle. Varying the incidence angle around the Bragg angle in what we term a rocking curve moves the SW vertically by one-half period, thus permitting the selective enhancement of photoemission from different depths in the sample. The inelastic attenuation of the photoelectrons also acts to enhance the standing-wave modulations near the top interface of any layer, such that even layers that are a few multilayer periods in thickness can still show rocking curve modulations, even if they will be smaller due to the effective sampling of more than one period. Beyond the modulations of photoelectron intensity due to Bragg reflection from the mirror, we also expect to see higher-frequency modulations often referred to as Kiessig fringes[25] due to reflection from the top of the mirror and the bottom of the mirror: these will be described by $m\lambda_x = D_{ML}\sin\theta_{inc}$, where D_{ML} is the total thickness of the multilayer mirror, and m is the order of interference. Further details on the theoretical background, the simulation program used for interpreting the data, and prior applications of this program to experiment, are found elsewhere.[7,9,26–28]

II. EXPERIMENTAL DETAILS

The experiment was carried out at the undulator beamline BL15XU of the SPring-8 synchrotron radiation facility (Hyogo, Japan). The x-ray energy was set to 5946 eV, and the incidence angle was about 2°, a choice which yields good spectral resolution and an x-ray penetration depth of about 1.8 μm. By contrast, the electron IMFPs quoted earlier imply an exponential decay of the elastically emitted electrons with a characteristic length of ≥80 Å.[10–12] The overall energy resolution (monochromator plus analyzer) was set to 250 meV, as verified by spectra of the Au valence band at the Fermi energy. The photoemitted electrons were detected and analyzed for their kinetic energy by means of a hemispherical analyzer (VG Scienta R4000). The angle between

the incident x-ray beam and the direction of the analyzer was 90°, and the incidence angle was grazing ($\vartheta_{inc} \approx 2°$), so that the photoelectrons were emitted approximately normal to the sample surface. The x-ray beam is p polarized, which means that the electric field vector is in the plane of incidence and is pointing only 2° away from the central lens axis of the electron spectrometer.

The analyzed sample consists of a synthetic multilayer mirror of 70 alternating layers of Si and Mo with thicknesses of 25.5 Å and 4.5 Å, respectively, with Si the topmost layer, grown on a polished and atmosphere-oxidized silicon substrate. It is reasonable to assume that the thin Mo layers of only about 1.5 unit cells in thickness do not remain as Mo metal but form a silicide film, and based on literature data it forms $MoSi_2$.[24] For the interpretation of the XPS and SW data, we thus assume that instead of Mo layers, the mirror consists of alternating layers of Si and $MoSi_2$. In addition, since the mirror had been exposed to air before the TiN deposition, a layer of native SiO_x had formed. No attempt was made to clean or alter this native oxide layer, but its presence was allowed for the analysis of the SW data. On top of this mirror, a layer of nominally 100 Å thick TiN was grown by a PVD process (Figure 1).

Before depositing the TiN film and attempting the SW-HXPS experiment, the multilayer mirror was characterized by hard x-ray diffraction in a separate diffractometer. The diffraction data confirm that the mirror consists of a total bilayer thickness of 30.0 Å, corresponding to the alternating layers of 25.5 Å of Si and 4.5 Å of $MoSi_2$. The interdiffusion at the interfaces of the bilayer was determined from an analysis of this hard x-ray diffraction data to be ≈2.5 Å, or about one atomic layer. The mirror is thus verified to be of high quality.

As noted above, the SW-XPS experiment involves first setting up a strong SW by tuning the x-ray incidence angle to the 1st-order Bragg reflection of the mirror, and then scanning the incidence angle from well below to well above this angle. Such scans, referred to as rocking curves, lead to a vertical movement of the SW by about one-half cycle through the TiN sample grown on top of the mirror. This results in strong modulations of the relative photoelectron intensities of XPS core peaks from elements at different depths below the surface.[29] Furthermore, the vertical period of the SW is equal to the total bilayer thickness of 30 Å. This period is thus very large compared to that in single-crystal Bragg-reflection SW-XPS experiments in which the periods are equal to typical interplanar distances or only a few Å.[30] The present method thus permits extending SW studies to thicker nm-scale multilayer structures, as relevant to many current applications, with recent reviews aimed at spintronics systems appearing elsewhere.

Some typical HXPS spectra are shown in Figure 2, which includes a broad survey spectrum in (a) and zoomed regions of Si 2s and Si 1s in (b) and (c), respectively. The oxidation of Si is seen in both the Si 2s and Si 1s spectra as a chemically shifted peak at higher binding energy (BE). Beyond this, the individual core-level spectra of Si 1s, N 1s, Ti 2p, O 1s, and Mo 3p were measured as a function of

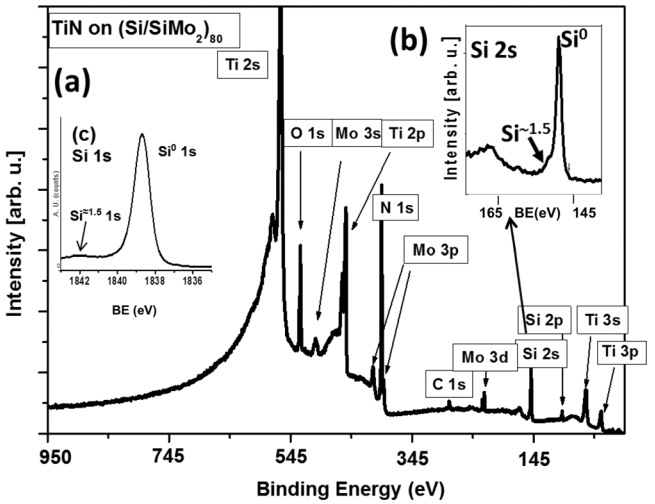

FIG. 2. (a) The broad XPS survey spectrum is shown with all major peaks labeled; (b) the inset is the detailed region from 146 to 160 eV of the Si 2s core level peak. Si 2s clearly shows the peaks of elemental Si ($Si2s^0$) and the sub-oxide Si $2s^{1.5}$, with x ≈ 1.5 based on past studies; (c) the inset is the Si 1s as a sum over all the angles. Si 1s collected at different angles has been used for obtaining the Si^0 and Si^{x+} rocking curves.

incidence angle to derive rocking curves. Peak intensities were determined by first subtracting a Shirley background[31] from the spectra and then fitting the peaks by Voigt functions, using software in the Igor Pro 6.21 environment.[32] These data have been collected while keeping the energy of the x-ray beam constant at 5946 eV and scanning the incidence angle of the x-rays from 1.86° to 2.22°. The step size between angles was set at 0.005° to allow for a reasonable number of data points in the sharp Bragg diffraction region, which has a theoretical full width half maximum of only 0.025° as determined from the calculated reflectivity curve,[33,34] in good agreement with our experimental results. The Bragg feature in reflectivity is observed at an angle of $\theta \approx 2.02°$ as a clear peak and a rapid intensity modulation in the vicinity of this angle.

Figure 3 shows a color-coded plot of the angular dependence of XPS spectra between binding energies of 370 eV and 600 eV which includes the Mo 3p, Mo 3s, N 1s, O 1s, Ti 2p, and Ti 2s core peaks. It is obvious that all of these peaks show strong modulation as the angle moves over the Bragg angle. Overlaid on this is a single spectrum obtained as a sum over all angles. The N 1s core level is affected by the presence of the weaker Mo $3p_{3/2}$ at 393 eV which partly overlaps it, but it can nonetheless be distinguished with fitting. Our subsequent XPS data analysis is focused on Mo 3p, O 1s, Ti 2p, and Si 1s, with similar angle-dependent chemical-state resolved spectra for O 1s, Ti 2p, and Si 1s being shown in Figure 4, with different chemical species assignments indicated. Our final experimental rocking curves for all four peaks studied are displayed as the points-with-curves in Figure 5. The rocking curves were simulated using the YXRO program developed by Yang that includes all relevant x-ray optical effects, i.e., the electron inelastic mean free paths, the refraction/reflection at the surface and buried interfaces, and the differential cross sections of the core levels of the various chemical species present.[7] This program has been used successfully in a

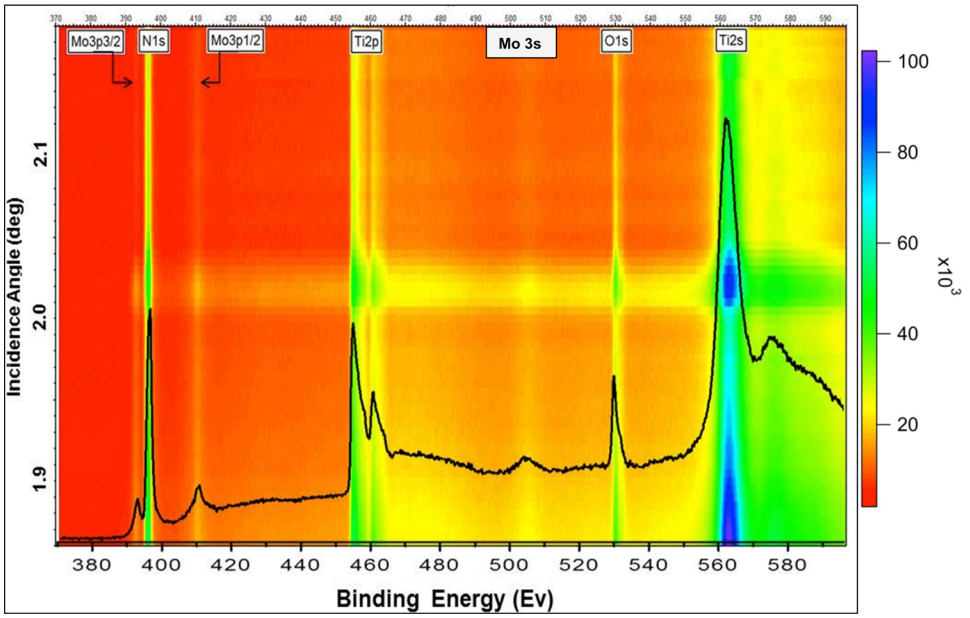

FIG. 3. Color plot of HXPS spectrum shown Mo 3p; N 1s; Ti 2p; Mo 3s, O 1s, Ti 2s core levels. The ordinate axes show the angles scanned in the range from 1.86° to 2.22° of the incident angle of the x-rays, and the abscissa shows the binding energy in eV. The spectrum here reported is the sum over all angles.

number of prior standing-wave photoemission and x-ray emission studies.[7,9,26–28]

The comparative soft XPS Ar^+ sputter depth profile data were obtained in the DTCL laboratory of Applied Materials in Santa Clara, CA. The sample was Ar^+ sputtered at energy of 1 keV, and a current of 1 μA and with a raster area of 2 mm × 2 mm for 10 s and subsequently the XPS spectra of the relevant core levels were collected with a laboratory Al Kα x-ray source at 1.5 keV. This was then repeated as the TiN was ion-etched into the Si. These are standard conditions for the sputter-profile analysis of such semiconductor layers.

III. RESULTS AND DISCUSSION

A. Hard x-ray standing-wave photoemission (SW-HXPS)

1. Experimental photoemission spectra and rocking curves

In Figure 4, the O 1s spectrum shows two separate peaks at BEs of ≈529.8 eV (labeled as O1) and ≈531.7 eV (labeled as O2). The Ti 2p spectrum shows the typical spin-orbit splitting of Ti $2p_{3/2}$ at BE ≈ 455 eV and Ti $2p_{1/2}$ at BE ≈ 460 eV. Both Ti $2p_{3/2}$ and Ti $2p_{1/2}$ peaks show a shoulder on the higher binding energy side (BE ≈ 457.6 eV and BE ≈ 462.7 eV, respectively) which can be attributed to the presence of a multi-electron screening satellite, or to a partly oxidized TiN (labeled provisionally as TiNO). Based on the energy position alone, a clear identification of this shoulder as either the satellite of the Ti 2p main peak (Ti 2p in TiN) or a peak originating from Ti 2p in the TiON layer is not possible. However, SW-HXPS is the perfect technique for solving this problem. In fact, if this shoulder is a multi-electron satellite of Ti 2p in TiN, the modulation of its rocking-curve should be the same as that of the main Ti 2p peak, because both the satellite and the main Ti 2p peaks originate from the same TiN layer and are part of the fundamental core photoemission process. On the other hand, if this shoulder is due to partly oxidized TiN, as the presence of the two O 1s components might suggest, it is likely that this TiO_xN_y layer forms at the top of the TiN layer due to air exposure of the sample. In this case, the shoulders at BE ≈ 457.6 eV and BE ≈ 462.7 eV assigned to Ti 2p in a TiNO environment should show a different rocking curve modulation from that of the main Ti 2p peaks in the TiN layer. As discussed in the next paragraph, SW-HXPS results clearly resolve this important issue in favor of the TiON assignment.

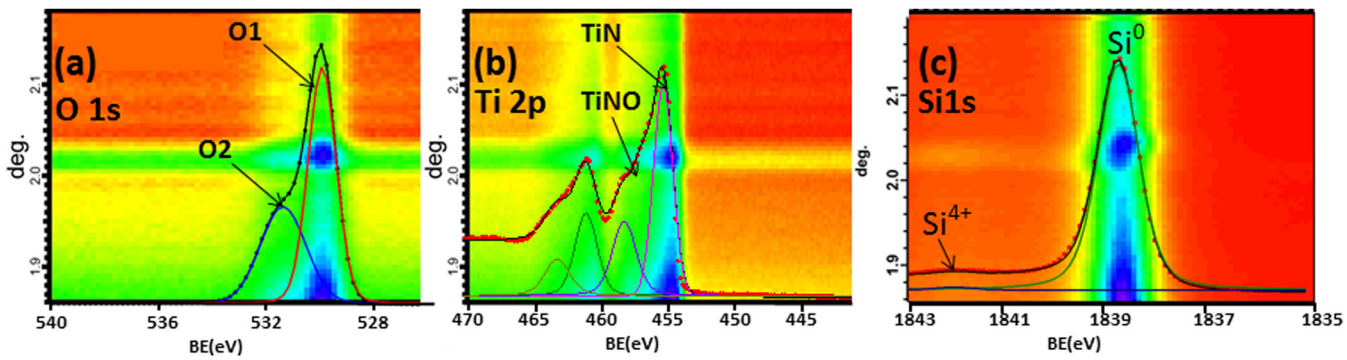

FIG. 4. Color code plot and curve fitting O 1s, Ti 2p, and Si 1s. The spectrum is the sum over all the angles.

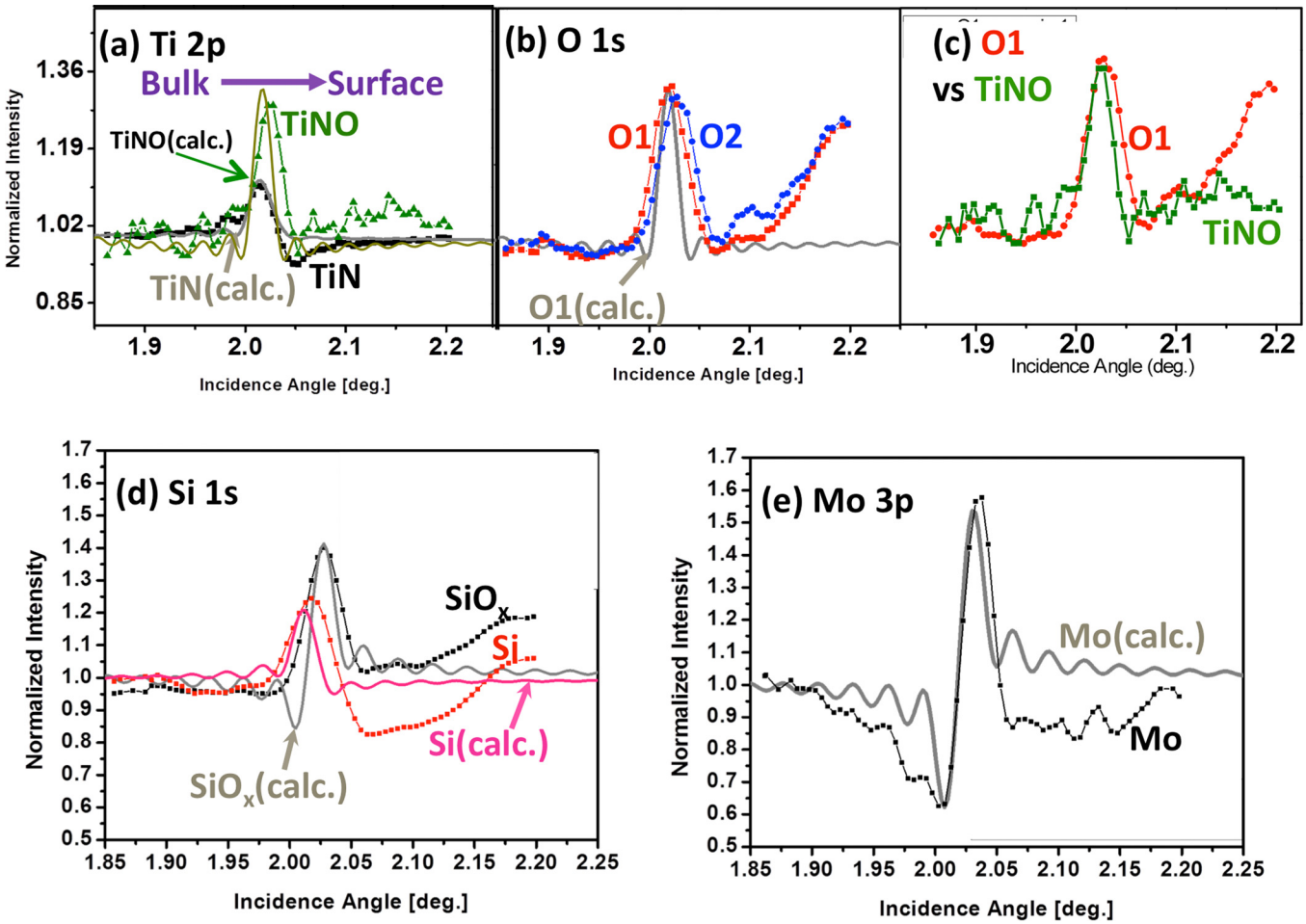

FIG. 5. Rocking curve data (lines with symbols) and x-ray optical simulations (solid lines) of the standing wave XPS experiment. In panels (a) and (b) are shown the normalized rocking curves of the Ti 2p and O 1s peaks, and in the panel (c) that of O 1s at BE ≈ 530 eV and of the Ti 2p shoulder at BE ≈ 47.6 eV for comparison. In panels (d) and (e) are shown the rocking curves of the multilayer elements: Si 1s and Mo 3p, respectively.

Figure 5 shows the normalized rocking curves of (a) Ti 2p and (b) O 1s that we expect to be associated with the topmost TiN layer, together with those of (d) Si 1s and (e) Mo 3p which represent the components of the multilayer mirror. Figure 5(c) also compares the experimental rocking curves from two components of Ti 2p and O 1s that we discuss in more detail below. Together with the experimental rocking curves, we also show calculated rocking curves obtained using the YXRO program mentioned previously.[7,29] We begin by discussing the experimental rocking curves obtained in the SW-HXPS data and then we compare them to the simulations.

The experimental rocking curves in Figure 5(a) of the Ti $2p_{3/2}$ component labeled TiON at BE ≈ 457.6 eV and of the main Ti $2p_{3/2}$ component at BE ≈ 455.0 eV show a marked difference in modulation and intensity. This means that the Ti atoms associated with these peaks originate from different depth distributions, and that the TiON component cannot be due to a multi-electron screening satellite of the main peak. Both simple two-wave modeling and fully quantitative calculations with the YXRO program[29] show that the standing wave moves towards the surface with increasing incidence angle. Thus, we can conclude from the fact that the TiON curve is shifted to the right relative to Ti that the TiON is on top of the TiN, as indicated by the arrow in the figure. The assignment of peak TiON to oxidized TiN is further supported by the fact that the binding energy of this component is shifted to higher values typical of an oxidized Ti contribution.[21] The rocking curves in Figure 5(b) for the two types of O 1s do not show as a dramatic difference, but there is definitely a slight shift to higher angles of that of O2 relative to O1, and a difference in the behavior of O2 at higher angles. The shift also implies via the argument used in Figure 5(a) that O2 represents atoms nearer to or at the surface; the fact that it is weaker compared to O1 also suggests that it is due to a final layer of adsorbed H_2O, CO, or other residual gases in the vacuum system. In addition, the rocking curve of O1 and that of TiON shows a strong similarity, as indicated in Figure 5(c), suggesting very strongly that they belong to the same layer, and further confirming that TiON is due to Ti atoms in a TiON layer instead of a multi-electron satellite. The weaker intensity modulation of the main Ti 2p peak in the TiN layer (≈10% compared to about 30% for TiON) in Figure 5(a) is due to the large escape depth of the electrons and to the large layer thickness of the TiN (100 Å) in comparison to the SW-HXPS period (≈30 Å); thus the x-ray wave field effectively samples a greater extent of its phase, due to the greater IMFP in HXPS, thus in effect integrating out the modulations to some degree. The presence of a top layer consisting of TiON is also of course consistent with the

fact that the sample was exposed to air for a prolonged time before measurement (about one month). The fact that intensity modulation of the O1 species and that of the TiNO species is significantly stronger than that of the Ti species further suggests that the TiON layer is significantly thinner than the TiN layer.

Figures 5(d) and 5(e) now show the rocking-curves of the core levels originating in the multilayer: Si 1s and the Mo $3p_{3/2}$. For the Si 1s core level, two different species were identified, one of which can be assigned to the elemental Si in the multilayer, and the second one to a silicon sub-oxide, which builds up due to storage of the silicon terminated multilayer in air before deposition of TiN. The BE of the sub-oxide, with a chemical shift of ≈2.3 eV with respect to the elemental peak, corresponds to Si^{x+} with $x < 4$. We do not find any evidence of significant Si^{+4} with an expected chemical shift of ≈3.7 eV in either Si 2p or much more intense Si 2s spectra, as illustrated by the insets of Figure 2, suggesting that the deposition of TiN has reduced the native oxide layer.

Most of the literature data on silicon sub-oxide chemical shifts are reported for Si 2p, and to a lesser degree, Si 2s core level peaks,[35,36] as the Si 1s binding energy of 1838 eV precludes study with SXPS sources. So for comparison, Figure 2 shows a broad survey spectrum and the insets showing the detailed region of the Si 2s and Si 1s core level peaks of the multilayer, where clearly the components of Si $2s^0$ and Si $2s^{x+}$ are observed. The chemical shift here suggests $x \approx 1.5$. In the Si 1s data, the thinner SiO_2 signal from the interface between the multilayer and the TiN layer shows a stronger modulation than the non-oxidized silicon; again, this is expected based on the degree to which the phase variation of the standing wave is sampled by high kinetic energy photoelectrons with long IMFPs. Via the same reasoning, it is easy to understand why the Mo in the thin $MoSi_2$ layers leads to a strong modulation in the Mo $3p_{3/2}$ signal, while the thicker layer of Si shows a smaller modulation.

2. Calculated rocking curves

Although the experimental rocking curves have already provided considerable information on the nature of the different chemical species and the layer structure, we have in order to more quantitatively derive the sample morphology, compared them with simulated results using the program written by Yang *et al.*[7,29] This program includes all of the basic physics of photoemission: the form of the electric field intensity with depth, the differential photoelectric cross section for each subshell, and the inelastic attenuation of the photoelectrons as they leave the sample. The x-ray interactions with the multilayer and the overlying sample layers are treated in a fully dynamical way. In these calculations, both the thicknesses of various layers and the degree of diffusion between them at interfaces have been used as fitting parameters. The optimized fits of such calculations to the experimental data after searching a number of different structures are shown as solid gray lines in Figures 5(a)–5(e). Beginning with the multilayer, there is good agreement between the experimental and simulated data for the Mo $3p_{3/2}$ core level (Figure 5(e)) and for both the elemental and oxidized Si components (Figure 5(d)); this is especially noteworthy, as this part of the sample is buried under a nominally 100 Å thick layer of TiN. Note also that, for the Mo $3p_{3/2}$ core level photoemission in Figure 5(e), theory does an excellent job of predicting the so-called Kiessig[25] fringes that result from reflection from the top of the multilayer and the underlying substrate, including their spacing, which agrees very well with the experiment. Neglecting refraction effects, the spacing $\Delta\theta$ of these fringes is in first approximation given by $\Delta\theta \approx \lambda_x/(n\, d_{ML}) = 3.55 \times 10^5/[h\nu(\text{eV})\ n\ D_{ML}(\text{Å})]$ in units of degrees, where λ_x is the x-ray wavelength, n is the number of periods of the multilayer, D_{ML} is the multilayer period, and $h\nu$ is the x-ray energy. For our case, this yields $\Delta\theta \approx 0.028°$, which is in reasonably good agreement with the fine structure seen in both the experiment and theory, which show $\Delta\theta \approx 0.021°$.The remaining deviations between the experiment and theory might be due to the effect of unresolved chemical-state contributions in the XPS spectra. As described in Figures 2 and 5, HXPS data show the presence of two kinds of Si, the elemental Si of the mirror and SiO_x of its oxidized top surface in contact with the TiN. The optimized comparison of the theory to experiment indicates that the sub-oxide $SiO_{x\approx1.5}$ layer is about 15 Å thick, is as expected on top of the multilayer, and diffuses by 4 Å into the TiN layer, i.e., with an interface roughness of 4 Å. The peak in the $SiO_{x\approx1.5}$ rocking curve is also, as expected, shifted to higher angles, as consistent with being nearer to the surface (cf. Figure 5(a)).

As noted previously, the high degree of similarity of the simulation results of the O1 and Ti2p in TiON rocking curves in Figure 5(c) suggests that they belong to the same layer. We have assigned the second oxygen contribution O2 in Figure 5(a) to a contamination of the surface due to the exposure to air and residual gas in the vacuum system. Our optimized simulation yields a total thickness of 20 Å for the top TiNO (including both types of oxygen) and indicates that the oxidized TiN and the TiN layers have an inter-diffusion depth of about 10 Å (see Figure 6). The analysis of Ti 2 s, N 1s (not reported in the paper) gives results which are, within estimated error bars, equivalent to the results obtained by the Ti 2p and O 1s analysis. The optimized simulation of the TiN layer yields a value of 77 Å for its thickness. Summing a 20 Å surface layer of TiNO, a 20 Å interface diffusion (assumed to be linear) between this layer and TiN, and a smaller interface diffusion of 4 Å between TiN and the SiO_x below it, we arrive after allowing for the stoichiometry and the densities of these layers at total amounts of Ti and N that are fully consistent with the 100 Å that was initially deposited. The small deviations observed between the theory and the experiment might be related to inhomogeneities in the sample.

Figure 6 shows the final sample morphology derived by this fitting procedure. In summary, the TiN depth-resolved composition as determined by the SW-HXPS data analysis is as follows: the top 20 Å of the TiN film consists of Ti-O-N likely due to the TiN exposure to air; below this TiON layer there is an interface of ≈20 Å of non-stoichiometric Ti, O and N; then, there is 77 Å of stoichiometric TiN film. The interface between the TiN film and the SiO_2 substrate is not sharp but shows a region of about 4 Å thick consisting of TiNOSi. The native oxide underneath the TiN is SiO_x

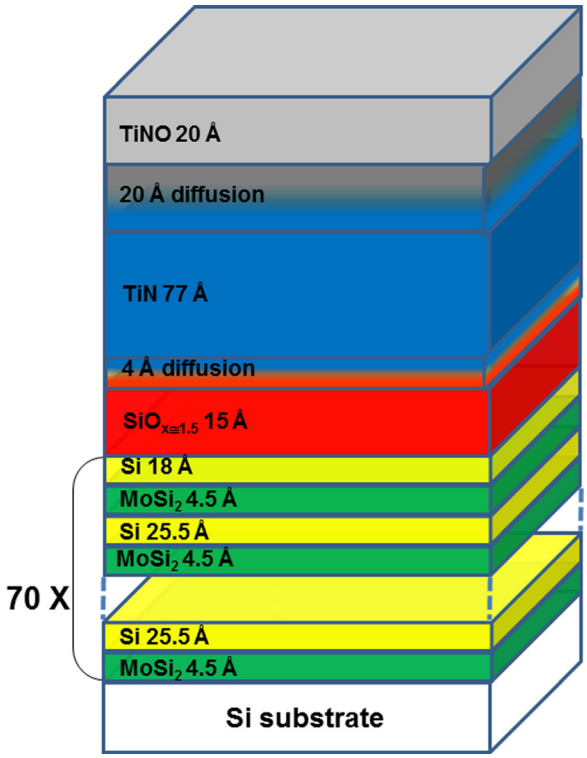

FIG. 6. The sample as determined from the final results of the standing-wave photoemission analysis. The multilayer consists of 70 bilayers of 25.5 Å Si and 4.5 Å of $MoSi_{\approx2}$. The nominal TiN thickness was given as 100 Å (cf. Fig. 1(b)).

($x \approx 1.5$) and is about 15 Å thick. As already mentioned, the oxygen content and its depth position are detrimental to the electrical properties of the TiN film. These results are thus significant from an applications point of view.

The possibility of accessing these deeply buried parts of the sample without any sample manipulation is very important for understanding the properties of layers grown on Si/SiO_2 substrates, since the thickness of the oxide, the chemical state distribution, and the interface roughness/intermixing determine the electrical properties of the layer above, as e.g., its leakage current, etc.[37] In fact, a great deal of effort is dedicated in the semiconductor industry to the quantitative characterization of buried interfaces. At present, TEM is the most popular technique used for this purpose; however, TEM analysis requires destructive sample preparation and the Si-O-N-Metal interface is in addition not easy to determine in a quantitative manner. This is the first time that a quantitative determination in term of thickness and stoichiometry of a buried SiO_x layer without sample alteration has been reported. This SW-HXPS method also allows us to verify the structure of the multilayer and to confirm the results from the x-ray diffraction measurements.

We now make a brief comparison of the SW-HXPS method to SXPS Ar^+ sputter depth profiling.

B. Sputter depth profile results

For comparison, Figure 7 shows the concentration profile resulting from an XPS Ar^+ sputter depth profile on an identical sample. The values are given in atomic percent. Before the

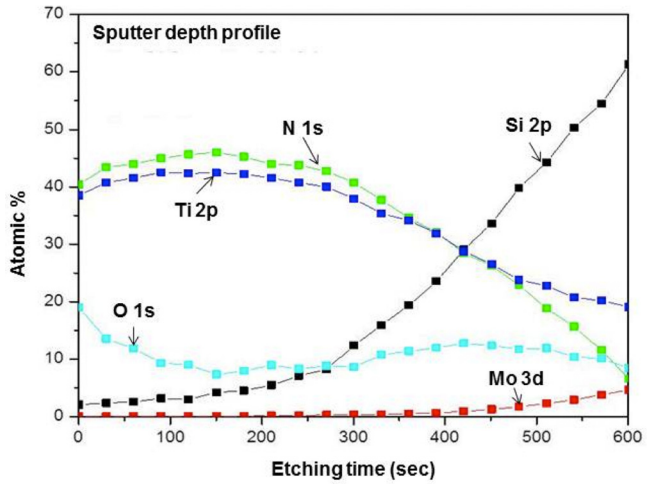

FIG. 7. Soft x-ray XPS depth profile obtained by Ar^+ ion sputtering. The x axis shows the etching time in seconds, the y axis shows the atomic percent of each element (Si, Ti, O, N, Mo).

sputtering process (etching time = 0), the sample shows equivalent amounts of Ti and N and a significant amount of O (O ≈ 20 at. %). After 100 s of Ar^+ sputtering, the Ti and N components increase due to the removal of the uppermost layer of oxygen containing contaminants originating from the exposure to air. Unfortunately, due to the inherent destructive process of sputtering (e.g., preferential sputtering and intermixing and possible alterations of the chemical identity of the layers), no chemical analysis of the peak profiles is possible. Up to 300 s of etching time, the layer still exhibits quite a large amount of oxygen (O ≈ 10 at. %, which might be due to re-adsorption of residual gas in the vacuum or to a differential sputtering effect) and a constant composition of Ti and N. As the TiN layer is reduced in thickness, the silicon and the molybdenum signal increase in intensity. After 300 s, the Si and the Mo contributions rise significantly, although Ti and N are still present. This suggests a strong intermixing of the multilayer and the TiN layer grown on top. A slight rise in the atomic percentage of oxygen suggests that there is SiO_x at the interface between TiN and the top of the multilayer, as observed also by SW-HXPS. After an etching time >400 s, the Si signal is predominant, but still Ti and N are found, although the amount of N is now lower than the amount of Ti. This might be an effect due to preferential sputtering, knock-on processes, or different diffusion into other layers.

A comparison of the Ar^+ sputtering depth profile and the SW-HXPS experiment leads to the conclusion that intermixing and preferential sputtering make it very hard to determine the exact chemical and structural properties of the TiN layer from the sputtering results, while the standing wave experiment clearly gives a quantitative description of the thickness of the layers, a more precise description of the structural parameters, including diffusion profiles and a more reliable determination of the chemical properties of deeper lying layers.

IV. CONCLUSIONS

In summary, a TiN layer grown on a Si/$MoSi_2$ multilayer was characterized by HXPS using the SW technique.

Core-level HXPS spectra for the different elements were measured as a function of incidence angle to generate rocking curve scans and these were analyzed both qualitatively and quantitatively using x-ray optical theory, thus leading to a precise description of the sample layers and interfaces. This analysis shows an oxidized first layer of 20 Å of TiNO that diffuses by 20 Å into a 77 Å thick TiN layer. This TiN layer is situated on the top of 15 Å of SiO_x (with $x \approx 1.5$) that originates from the storage of the multilayer mirror in air between its synthesis and the reducing effect of the TiN deposition. This deeply buried interface was accessible due to the high energy of the x-rays used.

A comparison of the XPS sputter depth profile and SW-HXPS data for the same sample shows the significantly greater ability of the SW-HXPS technique to provide accurate information on nanometer-scaled layered systems and their buried interfaces. Applications to many present device types are thus suggested. At present, the only limitation to use this technique as an industrial diagnostic method is that some of the multilayers available as substrates cannot be annealed for extended periods at $T > 200\,^{\circ}C$ in order to avoid the inter-diffusion of the layers, thus reducing their reflectivity. Such is the case for Mo/Si, in fact. However, recent tests of other binary combinations of materials such as W/C have shown stability for prolonged periods at up $800\,^{\circ}C$,[38,39] thus opening up the possibility of doing syntheses of samples under a wide range of more realistic semiconductor processing conditions.

ACKNOWLEDGMENTS

This work was supported by the Director, Office of Science, Office of Basic Energy Sciences, Materials Sciences and Engineering Division, of the U.S. Department of Energy under Contract No. DE-AC02-05CH11231. Two of us (CP and BB) also gratefully acknowledge the support of the Humboldt Foundation. The HXPES measurements were performed under the approval of NIMS Beamline Station (Proposal No. 2008A4906). This work was partially supported by the Nanotechnology Network Project, the Ministry of Education, Culture, Sports, Science and Technology (MEXT), Japan. The authors are grateful to HiSOR, Hiroshima University and JAEA/SPring-8 for the development of HXPES at BL15XU of SPring-8.

[1]J.-E. Sundgren, Thin Solid Films **128**, 21(1985).
[2]C. Y Ting and M. Wittmer, Thin Solid Films **96**, 327 (1982)
[3]E. Durğun Özben, J. M. J. Lopes, A. Nichau, R. Lupták, S. Lenk, A. Besmehn, K. K. Bourdelle, Q. T. Zhao, J. Schubert, and S. Mantl, J. Vac. Sci. Technol. B **29**, 01A903 (2011).
[4]A. Glaser, S. Surnev, F. P. Netzer, N. Fateh, G. A. Fontalvo, and C. Mitterer, Surf. Sci. **601**, 1153 (2007).
[5]J. Graciani, J. F. Sanz, T. Asaki, K. Nakamura, and J. A. Rodriguez, J. Chem. Phys. **126**, 244713 (2007).
[6]C. S. Fadley, Nucl. Instrum. Methods Phys. Res. A **547**, 24 (2005).
[7]S.-H. Yang, B. C. Sell, and C. S. Fadley, J. Appl. Phys. **103**, 07C519 (2008).
[8]S. Döring, F. Schönbohm, U. Berges, R. Schreiber, D. E. Bürgler, C. M. Schneider, M. Gorgoi, F. Schäfers, C. Papp, B. Balke, C. S. Fadley, and C. Westphal, Phys. Rev. B **83**, 165444 (2011).
[9]S. H. Yang, B. S. Mun, A. W. Kay, S. K. Kim, J. B. Kortright, J. H. Underwood, Z. Hussain, and C. S. Fadley, Surf. Sci. **461**, L557 (2000).
[10]S. Tanuma, C. J. Powell, and D. R. Penn, Surf. Interface Anal. **21**, 165 (1994).
[11]S. Tanuma, C. J. Powell, and D. R. Penn, Surf. Interface Anal. **43**, 689 (2011).
[12]QUASES-IMFP-TPP2M™ Software Package—version 2.1 Developed by S. Tougaard.
[13]S. Hofmann, Rep. Prog. Phys. **61**, 827 (1998).
[14]J. B. Price, J. O. Borland, and S. Selbrede, Thin Solid Films **236**, 311(1993).
[15]D. Deniz and J. M. E. Harper, J. Appl. Phys. **104**, 063519 (2008).
[16]A. Giardini, V. Marotta, S. Orlando, and G. P. Parisi, Surf. Coat. Technol. **151–152**, 316 (2002).
[17]K. Lal, A. K. Meikap, S. K. Chattopadhyay, S. K. Chatterjee, M. Ghosh, K. Baba, and R. Hatada, Physica B **307**, 150 (2001).
[18]T. S. Yeh, J. M. Wu, and L. J. Hu, Thin Solid Films **516**, 7294 (2008).
[19]B. Maiti, P. J. Tobin, C. Hobbs, R. I. Hegde, F. Huang, D. L. O'Meara, D. Jovanovic, M. Mendicino, J. Chen, D. Connelly, O. Adetutu, J. Mogab, J. Candelaria, and L. B. La, IEDM Tech. Dig. 781 (1998).
[20]Q. Guo, W. S. Oh, and D. W. Goodman, Surf. Sci. **437**, 49 (1999).
[21]I. Milošev, H. H. Strehblow, B. Navinšek, and P. Panjan, "Titanium nitride by XPS," Surf. Sci. Spectra **5**, 145 (1998).
[22]F. Sedona, G. A. Rizzi, S. Agnoli, F. X. Llabres i Xamena, A. Papageorgiou, D. Ostermann, M. Sambi, P. Finetti, K. Schierbaum, and G. Granozzi, J. Phys. Chem. B **109**, 24411 (2005).
[23]L. Porte, L. Roux, and J. Hanus, Phys. Rev. B **28**, 3214 (1983).
[24]D. G. Stearns, R. S. Rosen, and S. P. Vernon, Appl. Opt. **32**, 6952 (1993).
[25]H. Kiessig, Ann. Phys. **402**, 769 (1931).
[26]C. S. Fadley, S. H. Yang, B. S. Mun, J. Garcia de Abajo, in *Solid-State Photoemission and Related Methods: Theory and Experiment*, edited by W. Schattke and M. A. Van Hove (Wiley-VCH Verlag, Berlin GmbH, 2003), chap. 15.
[27]S. H. Yang, B. S. Mun, N. Mannella, A. Nambu, B. C. Sell, S. B. Ritchey, F. Salmassi, A. Schick, S. S. P. Parkin, and C. S. Fadley, J. Phys.: Condens. Matter **18**, L259 (2006).
[28]H. Yang, B. S. Mun, N. Mannella, S.-K. Kim, J. B. Kortright, J. Underwood, F. Salmassi, E. Arenholz, A. Young, Z. Hussain, M. A. V. Hove, and C. S. Fadley, J. Phys.: Condens. Matter **14**, L407 (2002).
[29]S.-H. Yang, A. X. Gray, A. M. Kaiser, B. S. Mun, J. B. Kortright, and C. S. Fadley, "Methodology and program for calculating x-ray optical effects with strong reflectivity in x-ray photo-emission and x-ray emission," J. Appl. Phys. (submitted).
[30]B. W. Batterman and H. Cole, Rev. Mod. Phys. **36**, 681(1964).
[31]D. A. Shirley, Phys. Rev. B **5**, 4709 (1972).
[32]IGOR PRO software package, WaveMetrics, Inc., Lake Oswego, Oregon, Igor Pro 6.2, 2010.
[33]B. L. Henke, E. M. Gullikson, and J. C. Davis, At. Data Nucl. Data Tables **54**, 181 (1993).
[34]V. G. Kohn, Phys. Status Solidi B **187**, 61 (1995).
[35]T. Eickhoff, V. Medicherla, and W. Drube, J. Electron Spectrosc. Relat. Phenom. **137–140**, 85 (2004).
[36]T. Hattori, H. Nohira, K. Azuma, K. W. Sakai, K. Nakajima, M. Suzuki, K. Kimura, Y. Sugita, E. Ikenaga, K. Kobayashi, Y. Takata, H. Kondo, and S. Zaima, Int. J. High Speed Electron. Syst. **16**, 353 (2006).
[37]D. K. Schroder, *Semiconductor Material and Device Characterization* (IEEE, 2006).
[38]C. Caspers, Juelich Research Center, private communication (June 2012).
[39]J. Gonzalez-Hernandez, B. S. Chao, D. A. Pawlik, D. D. Allred, and Q. Wang, J. Vac. Sci. Technol. A **10**, 145 (1992).